

---

# Efficient Trajectory Inference in Wasserstein Space Using Consecutive Averaging

---

**Amartya Banerjee**

Department of Computer Science  
University of North Carolina at Chapel Hill  
amartya1@cs.unc.edu

**Harlin Lee**

School of Data Science and Society  
University of North Carolina at Chapel Hill  
harlin@unc.edu

**Nir Sharon**

Department of Applied Mathematics  
Tel Aviv University  
nsharon@tauex.tau.ac.il

**Caroline Moosmüller**

Department of Mathematics  
University of North Carolina at Chapel Hill  
cmoosm@unc.edu

## Abstract

Capturing data from dynamic processes through cross-sectional measurements is seen in many fields such as computational biology. Trajectory inference deals with the challenge of reconstructing continuous processes from such observations. In this work, we propose methods for B-spline approximation and interpolation of point clouds through consecutive averaging that is intrinsic to the Wasserstein space. Combining subdivision schemes with optimal transport-based geodesic, our methods carry out trajectory inference at a chosen level of precision and smoothness, and can automatically handle scenarios where particles undergo division over time. We rigorously evaluate our method by providing convergence guarantees and testing it on simulated cell data characterized by bifurcations and merges, comparing its performance against state-of-the-art trajectory inference and interpolation methods. The results not only underscore the effectiveness of our method in inferring trajectories, but also highlight the benefit of performing interpolation and approximation that respect the inherent geometric properties of the data.

## 1 Introduction

Many dynamic processes yield cross-sectional observations at different timesteps, which can be represented as a sequence of *point clouds*, or discrete probability measures. To understand the underlying process, we need to first interpolate or approximate a likely path between these measurements. This problem of reconstructing continuous paths is called *trajectory inference*, which is seen in applications such as computational biology (Sha et al. [2023], Tong et al. [2020], Hugué et al. [2022], Schiebinger et al. [2019], Saelens et al. [2019]), computer graphics (Huang et al. [2022]), and control theory (Howe et al. [2022], Craig et al. [2024]). This paper considers the case where we only observe the state of a population as a whole, i.e. points in a point cloud do not have an inherent order. It may be the case that each sample is equivalent and interchangeable (e.g. drones in a swarm), or that there is no preservation of samples across time (e.g. cell measurement).

Recently, *optimal transport* (OT) (Peyré et al. [2019], Ambrosio et al. [2013], Villani [2008]) has shown to be effective in this problem, as it can provide a matching between two point clouds. By using OT to infer which sample at timestep  $t_i$  could correspond to which one at  $t_j$ , trajectories can be constructed in a way that minimize cost or effort. In the seminal work by Schiebinger et al. [2019], a piecewise linear OT interpolation method is proposed to infer cell trajectories. Higher order piecewise polynomials (e.g. cubic splines) were introduced in Chen et al. [2018], Benamou et al.

[2019] and extended by Chewi et al. [2021], Clancy and Suarez [2022], Justiniano et al. [2023]. Deep learning-based methods that try to fit smoother paths include TrajectoryNet (Tong et al. [2020]) and MIOFlow (Huguet et al. [2022]), which train neural ODEs with OT-informed tools.

Our paper fits in this line of work in the following sense. We propose a set of algorithms for trajectory inference (either interpolatory or approximate) on point clouds using consecutive OT-based geodesic averaging in the Wasserstein space. The methods are flexible and efficient as they allow us to tune the trajectories’ smoothness and accuracy. Furthermore, they are *intrinsic to the geometry of the Wasserstein space*, which naturally handles mass-splitting phenomena.

We first propose the *Wasserstein Lane-Riesenfeld (WLR)* algorithm to approximate B-splines in the Wasserstein space. We leverage the algorithm by Lane and Riesenfeld [1980], which efficiently defines B-splines in  $\mathbb{R}^d$  through consecutive averaging. It has been shown that this algorithm can be extended to Riemannian manifolds in Wallner and Dyn [2005], and our method extends this idea to the Wasserstein space by using a OT-based geodesic.

While the WLR algorithm is the main method we propose, we observe that consecutive averaging can be applied more broadly beyond B-splines, and following ideas from Wallner and Dyn [2005], we showcase an interpolatory trajectory inference method based on the 4-point scheme by Dyn et al. [1987]. We further discuss how our idea extends to any iterative method that uses consecutive averaging (e.g. any subdivision scheme).

Our contributions are:

1. Algorithmically, we define curves intrinsic to the Wasserstein geometry that do not depend on splines in  $\mathbb{R}^d$  as required in Chewi et al. [2021]. Our algorithms can therefore naturally deal with “trajectory splitting”, which is needed when mass is non-uniformly distributed over point clouds. This makes our methods comparable to other intrinsic Wasserstein spline methods, such as Chen et al. [2018], Benamou et al. [2019]. However, ours can be implemented easily and is more efficient when compared to those methods. Furthermore, our proposed algorithms can flexibly handle both approximation (via B-splines) and exact interpolation (via the 4-point scheme), and can be easily extended.
2. Theoretically, our approach is consistent with existing theory in degenerate cases. When each point cloud consists of just one point, we recover classical B-spline theory (on  $\mathbb{R}^d$ ). When there are only two point clouds, we recover the OT assignment between those point clouds. We also have convergence guarantees for the proposed algorithm.
3. Experimentally, WLR can accurately infer individual trajectories between uniform point clouds as for example needed in cell trajectories. WLR is fast and stable compared to deep-learning-based methods such as Tong et al. [2020], Huguet et al. [2022], subject to user’s choice of parameters; neural ODEs can fail under stiff dynamics or unstable optimization. WLR is however slightly slower than extrinsic methods such as Chewi et al. [2021], as we need to solve more OT problems than Chewi et al. [2021].

In the following sections, we describe background on optimal transport and splines (Sec. 2), state (Sec. 3) then demonstrate (Sec. 4) our proposed algorithms on various numerical experiments.

## 2 Preliminaries

We define relevant notations and formulate the trajectory inference problem, then present background on optimal transport and splines in the context of that problem. We view optimal transport as a special case of trajectory inference where there are only two point clouds, and splines in  $\mathbb{R}^d$  as another edge case where there is only one point per point cloud.

### 2.1 Problem formulation

We consider probability measures  $\mu_t$  over  $\mathbb{R}^d$  depending on a continuous time parameter  $t$ . For the purpose of implementation,  $\mu_t$  is a discrete probability measure or *point cloud*, i.e. it is defined by a set of support points  $x_t = \{x_{t,i}\}_{i=1}^{n_t} \subset \mathbb{R}^d$ , and a probability vector  $a_t \in \mathbb{R}_+^{n_t}$  with  $\sum_{i=1}^{n_t} a_{t,i} = 1$ . Mathematically, this can be described as  $\mu_t = \sum_{i=1}^{n_t} a_{t,i} \delta_{x_{t,i}}$ ; see Peyré et al. [2019]. Here,  $a_{t,i}$  describes the amount of mass located at  $x_{t,i}$ , and we allow for non-uniformly distributed mass.



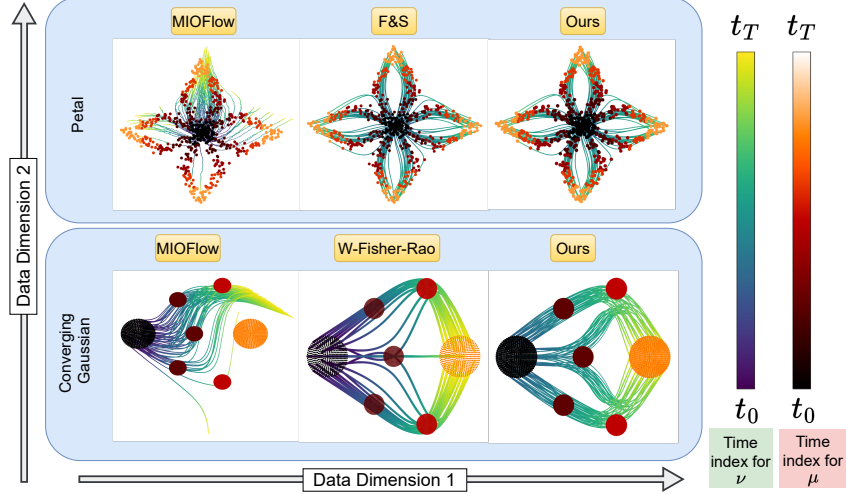


Figure 1: Our proposed WLR algorithm successfully performs trajectory inference on Petal (Top) and Converging Gaussian (Bottom) datasets. For Petal, the performances of F&S (Chewi et al. [2021]) and ours is similar since both use spline methods with data supported on  $\mathbb{R}^2$ . Despite our best efforts, we were not able to recreate the results for MIOFlow from Huguet et al. [2022]. For the Converging Gaussian, we compared our method to Wasserstein-Fisher-Rao splines by Clancy and Suarez [2022] (which performs unbalanced OT) since F&S cannot deal with splitting of masses and differing number of particles across timesteps. The fact that WLR can naturally deal with mass splitting phenomena is one of the major benefits. See Sec. 4 for more on these experiments.

Note that the number of points  $n_t$  may change at different times  $t$ , and while the points in  $x_t$  are inherently unordered, we give them an arbitrary yet consistent ordering and represent them as a matrix  $x_t \in \mathbb{R}^{d \times n_t}$  in a slight abuse of notation.

Given  $T + 1$  observations  $\mu_{t_0}, \dots, \mu_{t_T}$ , where  $t_0 < \dots < t_T$ , the aim of *trajectory inference* is to find probability measures  $\nu_t$  such that for  $j = 0, \dots, T$ ,  $\nu_{t_j} \approx \mu_{t_j}$  for approximation, or such that  $\nu_{t_j} = \mu_{t_j}$  for interpolation.

## 2.2 Discrete optimal transport and the Wasserstein space

In this section, we consider a single pair of point clouds  $(\mu_{t_0}, \mu_{t_1})$  as defined in Section 2.1. Discrete optimal transport (OT) studies the problem of transporting  $\mu_{t_0}$  to  $\mu_{t_1}$  in an “optimal” manner. Given a cost matrix  $C = [C_{ij}] \in \mathbb{R}_+^{n_{t_0} \times n_{t_1}}$  that describes how much effort is needed to move mass from one point in  $\mu_{t_0}$  to another in  $\mu_{t_1}$ , OT aims to find a coupling matrix  $\gamma \in \mathbb{R}_+^{n_{t_0} \times n_{t_1}}$  that attains

$$f := \min_{\gamma} \langle \gamma, C \rangle, \quad \text{where } \gamma \mathbf{1} = a_{t_0}, \gamma^\top \mathbf{1} = a_{t_1}, \gamma \geq 0. \quad (1)$$

Sometimes called the Kantorovich formulation, this equation by Kantorovich [2006] is often solved via linear programming. This has been crucial in applications including economics, inverse problems, image processing, computational biology, and most recently, machine learning (e.g. Courty et al. [2017]); see Peyré et al. [2019] for an excellent overview on computational OT. A popular choice for cost is  $C_{ij} = \|x_{t_0,i} - x_{t_1,j}\|^p$  for  $p \geq 1$ , in which case  $W_p(\mu_{t_0}, \mu_{t_1})$ , the  $p$ -Wasserstein distance between  $\mu_{t_0}$  and  $\mu_{t_1}$ , is defined as  $f^{1/p}$  using the minimum value attained in eq. (1).

When the space of probability measures on  $\mathbb{R}^d$  with finite  $p$ -th moment is equipped with  $W_p$ , we call it *Wasserstein space*. The Wasserstein space is a metric space and carries Riemannian-like structure. It can formally be considered an infinite dimensional Riemannian manifold (Otto [2001], Lott [2008]). Representing the point clouds to be on the Wasserstein space allows us to define useful geometric properties such as barycenters (Agueh and Carlier [2011]). Of particular interest to trajectory inference is the *geodesic* in the Wasserstein space. Once  $\gamma$  is obtained, the constant speed geodesic between  $\mu_{t_0}$  and  $\mu_{t_1}$  is given by the pushforward measure:

$$\mu_\alpha = (\pi_\alpha)_\# \gamma, \quad \text{where } \pi_\alpha(x_{t_0,i}, x_{t_1,j}) = (1 - \alpha)x_{t_0,i} + \alpha x_{t_1,j} \text{ and } \alpha \in [0, 1]. \quad (2)$$

By definition,  $\mu_\alpha$  is the shortest path between  $\mu_{t_0}$  and  $\mu_{t_1}$  in the Wasserstein space. See Villani [2008], Santambrogio [2015], Ambrosio et al. [2013] for more background on Wasserstein geometry.

### 2.3 Splines through consecutive averaging

We discuss another edge case of Section 2.1, namely where each point cloud only has a single point, that is,  $n_t = 1$ . Splines are popular methods that fit piecewise polynomial curves through such data points in  $\mathbb{R}^d$ . In this work, we limit our discussion of splines from the viewpoint of *subdivision schemes*. These are iterative refinement methods that approximate continuous or smooth curves based on a sequence of initial data points, which is also called knots. See Appendix A for details.

---

#### Algorithm 1 B-spline Approximation Algorithm by Lane and Riesenfeld [1980]

---

```

1: procedure LANERIESENFELD( $[x_j]_{j \in \mathbb{Z}}, R, M$ )
2:   input Points to be refined  $[x_j]_{j \in \mathbb{Z}}, x_j \in \mathbb{R}^d$ .
3:   input Refinement level  $R \in \mathbb{Z}_+$ .
4:   input Degree  $M$  of B-splines to be approximated.  $M = 3$  for cubic B-splines.
5:    $y^{(M)} \leftarrow [x_j]_{j \in \mathbb{Z}}$  ▷ Initializing points to be doubled.
6:   for  $r = 1$  to  $R$  do
7:     for  $j \in \mathbb{Z}$  do
8:        $y_{2j}^{(0)} \leftarrow y_j^{(M)}$  ▷ Doubling points.
9:        $y_{2j+1}^{(0)} \leftarrow y_j^{(M)}$ 
10:    end for
11:    for  $m = 1$  to  $M$  do
12:      for  $j \in \mathbb{Z}$  do
13:         $y_j^{(m)} \leftarrow \frac{1}{2}(y_j^{(m-1)} + y_{j+1}^{(m-1)})$  ▷ Repeated averaging.
14:      end for
15:    end for
16:  end for
17:  return Refined points  $[y_j^{(M)}]_{j \in \mathbb{Z}}$ .
18: end procedure

```

---

We focus on one such method by Lane and Riesenfeld [1980] in Algorithm 1. The Lane-Riesenfeld algorithm depends on two parameters, the degree  $M$ , which is related to the smoothness of the limit curve, and the refinement level  $R$ , which flexibly handles the accuracy of the approximation curve. As  $R \rightarrow \infty$ , we obtain a B-spline of degree  $M$  in  $\mathbb{R}^d$  which is  $C^{M-1}$  (Cavaretta et al. [1989]).

Algorithm 1 contains two main phases: doubling of points and computing averages between consecutive points. Following Wallner and Dyn [2005], Dyn and Sharon [2017a], we can generalize the averaging phase via a linear averaging operator between two points  $y_i, y_j \in \mathbb{R}^d$  and  $\alpha \in [0, 1]$ :

$$\text{av}_\alpha(y_i, y_j) = (1 - \alpha)y_i + \alpha y_j. \quad (3)$$

With this operator, step (13) of Algorithm 1 becomes  $y_j^{(m)} \leftarrow \text{av}_{1/2}(y_j^{(m-1)}, y_{j+1}^{(m-1)})$ . It has been observed that Algorithm 1 can be further adapted to work on finite-dimensional Riemannian manifolds by replacing  $\text{av}_\alpha$  with the geodesic average on the Riemannian manifold (Wallner and Dyn [2005]).

### 3 Wasserstein curve approximation through consecutive averaging

We have now gathered two ingredients for trajectory inference. On one hand, we have a way to calculate the shortest path between two point clouds in the Wasserstein space (Section 2.2). On the other hand, we have a way to efficiently fit a curve through many points in  $\mathbb{R}^d$  (not point *clouds*) from Section 2.3. Our key insight is that if we replace the linear averaging operator in eq. (3) with the Wasserstein geodesic in eq. (2), we can use the consecutive averaging approach described in Section 2.3 to define smooth approximating curves through the point clouds in the Wasserstein space.

We propose the Wasserstein Lane-Riesenfeld (WLR) algorithm (c.f. Algorithm 2), which parallels the ideas of Dyn and Sharon [2017b,a] and incorporates an OT-based averaging step (c.f. Algorithm 3). This adjustment preserves the algorithm’s simplicity and scalability at a given refinement level, while effectively tackling the task of B-spline approximation. The defining characteristic of WLR is that the resulting curve is *intrinsic* to the Wasserstein geometry since the geodesic averaging step stays within the Wasserstein space. This is similar to the computationally heavier algorithms of Chen et al. [2018],

but different from e.g. Chewi et al. [2021], which is *extrinsic* in the sense that it constructs splines in  $\mathbb{R}^d$ . An important consequence is that unlike prior work, WLR has the ability to automatically handle non-uniform mass, mass splitting and bifurcations.

---

**Algorithm 2** Ours: Wasserstein Lane-Riesenfeld (WLR)

---

```

1: procedure WASSERSTEIN-LANERIESENFELD( $[\mu_{t_j}]_{j=0}^T, R, M$ )
2:   input Point clouds to be refined  $[\mu_{t_j}]_{j=0}^T$ .
3:   input Refinement Level  $R \in \mathbb{Z}_+$ .
4:   input Degree  $M$  of B-Splines to be approximated.
5:    $\nu^{(M)} \leftarrow [\mu_{t_j}]_{j=0}^T$  ▷ Initializing point clouds to be doubled.
6:   for  $r = 1$  to  $R$  do
7:     for  $j = 0$  to  $|\nu^{(M)}|$  do
8:        $\nu_{2j}^{(0)} \leftarrow \nu_j^{(M)}$  ▷ Doubling point clouds.
9:        $\nu_{2j+1}^{(0)} \leftarrow \nu_j^{(M)}$ 
10:    end for
11:     $\nu^{(0)} \leftarrow [\underbrace{\nu_0^{(0)}, \dots, \nu_0^{(0)}}_{m \text{ times}}, \nu_1^{(0)}, \dots, \nu_{T-1}^{(0)}, \underbrace{\nu_T^{(0)}, \dots, \nu_T^{(0)}}_{m \text{ times}}]$ 
12:    for  $m = 1$  to  $M$  do
13:      for  $j = 0$  to  $|\nu^{(m-1)}|$  do
14:         $\nu_j^{(m)} \leftarrow \text{OT-av}(\nu_j^{(m-1)}, \nu_{j+1}^{(m-1)}, \frac{1}{2})$  ▷ Repeated OT averaging (Algorithm 3).
15:      end for
16:    end for
17:  end for
18:  return Refined point clouds  $\nu^{(M)}$ .  $|\nu^{(M)}| = 2^R(T + M - 1) + 2 - M$  in our implementation.
19: end procedure

```

---



---

**Algorithm 3** Optimal Transport Averaging via Wasserstein Space Geodesic in eq. (2)

---

```

1: procedure OT-AV( $\mu_A, \mu_B, \alpha$ )
2:   input First point cloud  $\mu_A: (x_A, a_A)$ .  $x_A$  has  $n_A$  points.
3:   input Second point cloud  $\mu_B: (x_B, a_B)$ .  $x_B$  has  $n_B$  points.
4:   input Averaging parameter  $\alpha \in [0, 1]$ .
5:    $\gamma \leftarrow \text{OT}(\mu_A, \mu_B)$  ▷ Solve eq. (1) via linear programming and obtain  $\gamma \in \mathbb{R}^{n_A \times n_B}$ .
6:    $x, a \leftarrow \text{null}$ 
7:   for  $i = 1$  to  $n_A$  do
8:     for  $j = 1$  to  $n_B$  do
9:       if  $\gamma_{i,j} > \epsilon$  then ▷  $\epsilon > 0$  is a chosen threshold.
10:        Column-wise concatenate  $(1 - \alpha) \cdot x_{A,i} + \alpha \cdot x_{B,j}$  to  $x$ .
11:        Append  $\gamma_{i,j}$  to  $a$ .
12:      end if
13:    end for
14:  end for
15:   $a \leftarrow a / \text{sum}(a)$  ▷ Renormalization.
16:  return Averaged point cloud  $\mu_\alpha$  defined by  $(x, a)$ .
17: end procedure

```

---

Before diving into numerical experiments, we illustrate our algorithm’s behavior on two dimensional toy data. Figure 2 plots three point clouds ordered (in time) from left to right. In the top row, all points have uniform mass. In the bottom row, mass is non-uniformly distributed in the second and third timesteps. This demonstrates the following capacities of WLR.

**Trajectory inference** WLR produces natural trajectories between point clouds. In our implementation of WLR, we repeat the end point clouds  $\mu_{t_0}$  and  $\mu_{t_T}$  before averaging (see (11) in Algorithm 2) so that they are interpolated. Therefore, when a sequence of point clouds  $\nu$  is returned by WLR, we can set the first point cloud as  $\nu_{t_0} = \mu_{t_0}$ , the last point cloud as  $\nu_{t_T} = \mu_{t_T}$ , and evenly space out the remaining point clouds in between  $t_0, t_1, \dots, t_T$ . In addition, if we compute OT between

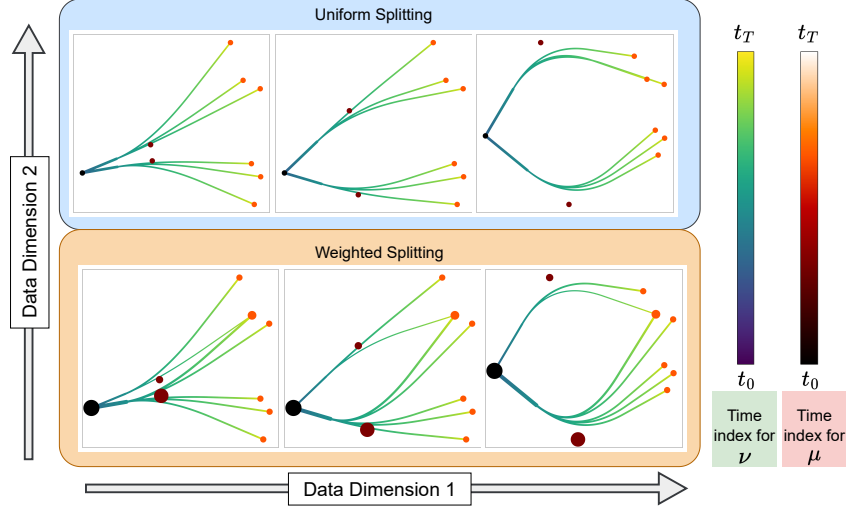


Figure 2: WLR approximation on three point clouds in  $\mathbb{R}^2$  with uniform (Top) and non-uniform (Bottom) mass. The size of the point is proportional to  $a_{t_j, i}$ , the mass of point  $i$  at timestep  $t_j$ . In all cases, the trajectories respect the geometry of the Wasserstein space.

consecutive pairs of point clouds in  $\nu$ , we are able to trace how mass from a single point in  $\mu_{t_0}$ , i.e. mass of weight  $a_{t_0, i}$  supported on  $x_{t_0, i}$ , travels from  $t_0$  to  $t_T$ . In other words, we are able to trace trajectories of individual samples in  $\mathbb{R}^d$  over time.

**Approximation and bending behavior** B-splines in  $\mathbb{R}^d$  do not interpolate given data. Rather, they find an approximating path between the knots. Figure 2 shows that this is still true for WLR and how the points in the second timestep “bend” the trajectories like gravitational objects, and the bending is weighted by the mass located in each of the points.

**Splitting trajectories** This phenomenon naturally occurs in point clouds with non-uniform weights. Our algorithm can accommodate this automatically through the geodesic averaging procedure.

Lastly, we note that OT-based geodesic averaging can be applied to subdivision schemes beyond B-splines. Following ideas from Wallner and Dyn [2005], we describe an interpolatory trajectory inference method based on the 4-point scheme by Dyn et al. [1987] in Appendix A.1.

### 3.1 Complexity analysis

WLR’s runtime depends on the B-spline degree  $M$ , number of initial point clouds  $T + 1$ , refinement level  $R$ , and number of points per point cloud  $n_t$ . If the number of points stay the same, i.e.  $n_t = n$ , and there is a one-to-one mapping at each OT step, the overall complexity of WLR is  $\mathcal{O}(2^R \cdot (T + M) \cdot n^3 \cdot \log n)$ . Naturally, computation increases as  $M$  (indicating smoothness) and  $R$  (indicating approximation accuracy) increase. It is important to note that in the subdivision scheme literature,  $R$  is no greater than 8 and  $M = 3$  suffice for most visual purposes. Still we provide a careful study of the interplay between these parameters for WLR runtime in Appendix B.

The most time consuming procedure is computing discrete OT in (5) of Algorithm 3, for which we use linear programming implemented in Python OT (Flamary et al. [2021]). In practice, we also vectorize lines (7-14) in Algorithm 3. Since the averaging operations only happen between consecutive point clouds, it is theoretically possible to parallelize WLR, but we leave that for future work.

### 3.2 Convergence analysis

For the purpose of the convergence proof, we consider the data  $\mu_{t_j}, j = 0, \dots, T$  in the  $p$ -Wasserstein space over  $\mathbb{R}^d$ ,  $\mathcal{W}_p(\mathbb{R}^d)$ , which is the space of all probability measure with finite  $p$ -th moment. This space is a metric space with distance given by the  $p$ -Wasserstein distance  $W_p$  in Section 2.2.

The  $p$ -Wasserstein distance satisfies the geodesic property: for any two measures,  $\mu_i$  and  $\mu_j$  we have

$$W_p(\text{OT-av}_\alpha(\mu_i, \mu_j), \mu_j) = (1 - \alpha) W_p(\mu_i, \mu_j), \quad \alpha \in [0, 1]. \quad (4)$$

In addition,  $\mathcal{W}_p(\mathbb{R}^d)$  is a separable complete metric space since  $\mathbb{R}^d$  has these properties (Villani [2008]). Therefore, any Cauchy sequence in  $\mathcal{W}_p(\mathbb{R}^d)$  converges, which is the main property we need for the following convergence result.

Our subdivision scheme (WLR) generates sequences of point clouds, starting from the initial data  $\nu^{(0)} = [\nu_{t_j}^{(0)}]_{j=0}^T$  with  $\nu_{t_j}^{(0)} = \mu_{t_j}$ , and generating, by repeated refinements, the sequences  $\nu^{(R)} = [\nu_j^{(R)}]_{j=0}^{2^{R,T}+1}$ ,  $R \in \mathbb{N}$ . Therefore, informally, the limit  $\nu = \lim_{R \rightarrow \infty} \nu^{(R)}$  is the object we seek in Section 2.1. Technically, we associate each refinement level’s data  $[(j2^{-R}, \nu_j^{(R)})]_{j=0}^{2^{R,T}+1}$  with the piecewise geodesic interpolant in  $\mathcal{W}_p(\mathbb{R}^d)$ , which is defined using the Wasserstein geodesic of eq. (2) and is calculated by Algorithm 3. The piecewise geodesic interpolant is

$$N^{(R)}(t) = \text{OT-av}_t(\nu_i^{(R)}, \nu_{i+1}^{(R)}), \quad t \in [i2^{-R}, (i+1)2^{-R}).$$

Then, the refinement scheme (e.g. WLR) is called convergent if the sequence of piecewise geodesic interpolants  $\{N^{(R)}(t)\}_{R \in \mathbb{Z}_+}$  converges uniformly (in  $t$ ) to a limit curve, where the curve takes values in the Wasserstein space  $\mathcal{W}_p(\mathbb{R}^d)$ . This is called the *limit of the subdivision scheme*.

The result for our WLR schemes reads:

**Theorem 1.** *Consider a sequence of measures  $\mu_{t_0}, \dots, \mu_{t_T}$  with  $t_0 < \dots < t_T$ . Define the initial data by  $\nu^{(0)} = [\nu_{t_j}^{(0)}]_{j=0}^T$  with  $\nu_{t_j}^{(0)} = \mu_{t_j}$ , and choose a smoothness degree  $M$ . Apply WLR (i.e. call Algorithm 2 for the initial data, smoothness  $M$ , and refinement level  $R$ ) to obtain a  $R$ -times refined sequence of measures  $\nu^{(R)}$ . As  $R \rightarrow \infty$ , WLR converges to a continuous limit curve  $\nu$  in  $\mathcal{W}_p(\mathbb{R}^d)$ , where convergence is in the sense of subdivision schemes defined above.*

The proof follows from [Dyn and Sharon, 2017b, Corollary 3.3]. An outline of the proof’s main arguments is given for completeness in Appendix C.

## 4 Experiments

We conduct trajectory inference on simulated data to compare the effectiveness of WLR against other state-of-the-art algorithms: MIOFlow (Huguet et al. [2022]), TrajectoryNet (Tong et al. [2020]), F&S (Chewi et al. [2021])<sup>1</sup>, and Wasserstein-Fisher-Rao (Clancy and Suarez [2022]). We first perform trajectory inference using all timesteps in the datasets and visualize WLR trajectories in Figure 3. Due to the page limit, full visualization of other methods are deferred to Figure 6 in Appendix D, but readers can refer back to Figure 1 for selected examples. In addition, we quantitatively assess our method by interpolating omitted timepoints as suggested in Huguet et al. [2022]. Specifically, for each algorithm, we withhold data at a common intermediate timestep during the ‘training’ phase. In the ‘inference’ phase, we predict the outcomes for the omitted timestep and document the 1-Wasserstein ( $W_1$ ) distance and the Mean Squared Error (MSE) between the predicted and the omitted point clouds. We hold out timesteps in a manner that makes the task the most difficult. Additionally, we calculate the average  $W_1$  distance and MSE across all timesteps. These findings are reported in Table 1. Our Python code is available at <sup>2</sup>. When possible, we optimized code and tuned parameters of other methods for fair comparison. See Appendix E for more on experimental setup and dataset sizes.

### 4.1 Datasets

We use a wide range of simulated datasets that replicate the natural dynamics observed in cellular differentiation. This includes phenomena such as bifurcations and merges, as depicted in Figure 3.

**Diverging Gaussian** We designed this dataset (Figure 3a) to initiate from a singular point cluster and gradually disperse as time progresses. The points all have uniform mass.

<sup>1</sup>The original paper only considers cubic spline interpolation in  $\mathbb{R}^d$ , but we extended their algorithm to B-spline approximation in  $\mathbb{R}^d$  via Lane-Riesenfeld algorithm for a fair comparison.

<sup>2</sup>To be replaced with a Github link after peer review.

**Petal** The Petal dataset (Figure 3b), as defined by Hugu et al. [2022], presents a significant challenge due to its inherent geometric structure. We resampled it to make  $n_t$  consistent. The points all have uniform mass.

**Converging Gaussian** This dataset (Figure 3c) was crafted by Clancy and Suarez [2022] to simulate the intricate dynamics characteristic of cellular differentiation. The points are sampled from Gaussian distributions with intermediate stages having cellular division processes. Changing  $n_t$  across intermediate timesteps makes this dataset challenging. F&S cannot handle this setup, so we skip it. On the other hand, we were not able to adapt code by Clancy and Suarez [2022] to run on any other datasets, so we report results from Wasserstein-Fisher-Rao only on Converging Gaussian. We also do not calculate MSE since the definition becomes ambiguous as the number of points between the predicted point clouds and the held out point clouds can differ.

**Dyngen Tree and Cycle** Utilizing Dyngen by Cannoodt et al. [2021], we simulated a single-cell RNA sequencing (scRNA-seq) dataset to model a dynamic cellular process. We generated both tree (Figure 3d) and cycle (Figure 3e) data, using 100 transcription factors for each. They were then embedded into a 10-dimensional space via PCA and PHATE (Moon et al. [2019]), respectively.

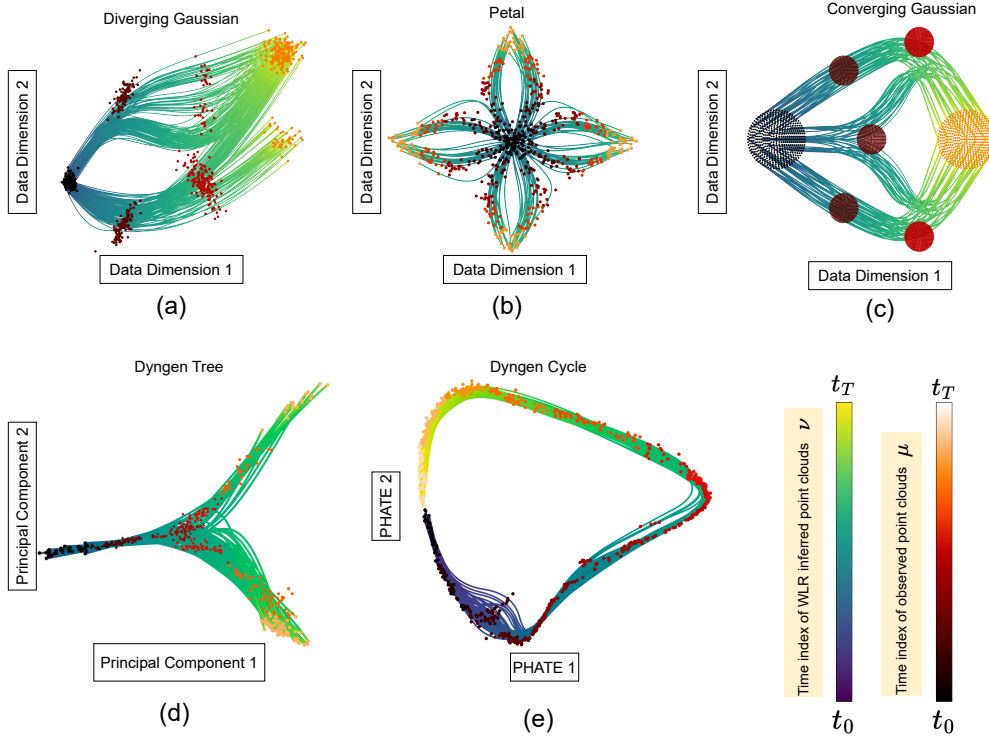


Figure 3: WLR produces smooth and visually convincing trajectories on five synthetic datasets that mimic cell differentiation. For both Dyngen datasets, the trajectory inference is done in the 10-dimensional space.

## 4.2 Discussion

Table 1 and Figure 3 suggest that our method performs consistently well across various datasets in terms of runtime,  $W_1$  distance and MSE, as well as producing visually convincing, smooth curves. It is clear from Table 1 and Figure 6 (or selected examples in Figure 1) that the deep learning-based methods suffer from long training time and unstable optimization. For example, in Petal and Converging Gaussian, we observe that MIOFlow produces trajectories that are heavily concentrated in some areas and sparse in others, and the paths do not consistently move in a clear direction from one timestep to another, leading to ambiguity in the inferred trajectories.

Table 1: WLR consistently performs **best** or **second best** on predicting point clouds at omitted timesteps.

Dataset	Method	Held out timestep	Runtime (sec) ↓	Leave-one-out		Mean	
				MSE ↓	$W_1$ ↓	MSE ↓	$W_1$ ↓
Diverging Gaussian	WLR (Ours)	$j = 2$	3.243	<b>0.940</b>	1.150	<b>0.437</b>	0.603
	MIOFlow		43.122	1.880	<b>0.852</b>	2.029	0.877
	TrajectoryNet		1238.30	17.311	5.829	13.296	4.871
	F & S		<b>0.925</b>	1.664	<u>1.309</u>	<u>0.981</u>	<b>0.586</b>
Petal	WLR (Ours)	$j = 2$	19.248	<b>0.008</b>	<b>0.114</b>	<b>0.015</b>	0.113
	MIOFlow		55.379	0.336	0.199	0.358	0.152
	TrajectoryNet		1643.12	1.451	1.016	<u>0.186</u>	0.298
	F & S		<b>9.159</b>	<u>0.294</u>	<u>0.115</u>	0.369	<b>0.091</b>
Converging Gaussian	WLR (Ours)	$j = 2$	<b>0.898</b>	-	<b>0.693</b>	-	<b>0.288</b>
	MIOFlow		<u>42.453</u>	-	0.978	-	<u>0.471</u>
	TrajectoryNet		1402.05	-	2.208	-	2.098
	F & S		-	-	-	-	-
Dyngen Tree	WLR (Ours)	$j = 3$	<u>15.010</u>	<b>0.798</b>	<u>1.794</u>	<b>0.595</b>	<b>1.323</b>
	MIOFlow		16.584	1.103	2.536	3.734	4.603
	TrajectoryNet		4316.89	1.456	3.256	2.328	3.465
	F & S		<b>6.895</b>	<u>0.807</u>	<b>1.787</b>	<u>1.712</u>	<u>1.710</u>
Dyngen Cycle	WLR (Ours)	$j = 8$	<u>1.901</u>	<b>0.049</b>	<b>0.579</b>	<b>0.067</b>	<b>0.733</b>
	MIOFlow		36.078	0.325	1.731	0.532	2.183
	TrajectoryNet		11298.64	21.615	14.693	10.254	9.157
	F & S		<b>1.649</b>	<u>0.064</u>	<u>0.667</u>	<u>0.085</u>	<u>0.870</u>

F&S exhibits the shortest runtime in all instances, and often produces second best results to WLR both quantitatively and qualitatively. In the case of Diverging Gaussian and Petal, F&S and WLR trajectories look identical to the human eye. However, a significant drawback is that it fundamentally lacks the ability to handle mass splitting and having differing number of particles across timesteps, e.g. Converging Gaussian.

The Wasserstein-Fisher-Rao splines extend F&S to the mass splitting case including Converging Gaussian. In fact, they introduced the Converging Gaussian dataset, and hence provide an authoritative baseline for our evaluation. Wasserstein-Fisher-Rao splines provide distinct paths and appears to be an improvement from deep learning-based methods. However, some of the trajectories cross each other between the first and second timesteps, and some also ignore the third timestep and jump straight from second to the last timestep. These paths are not ‘optimal’ in the sense of optimal transport, and could lead to misinterpretation of how points are moving between timesteps.

Overall, WLR dependably produces trajectories that are natural (as seen in visualizations) and accurate (as measured by predicting held-out point clouds).

## 5 Conclusions

We present a simple framework for trajectory inference on point clouds that respects the inherent geometry in the data. Our method builds on subdivision scheme methods with optimal transport-based geodesic to efficiently and provably approximate (or interpolate) curves in the Wasserstein space. Unlike prior work based on neural ODEs, which may fail under stiff dynamics or rely heavily on hyperparameters, our method consistently provides smooth and accurate trajectories in a user-controlled way. Moreover, we posit that employing our framework as an initialization step could enhance the convergence rates of various neural network-based trajectory inference methods.

## 6 Limitations and Broader Impact

Our proposed methods have the following limitations, which we plan to address in future work. (1) The WLR algorithm works best with sparse OT solutions, i.e. solving a linear program as we outlined. Using approximation schemes such as the Sinkhorn algorithm of Cuturi [2013] leads to many lightly weighted trajectories which blow up computations. A hard threshold might be able to mitigate this problem. (2) While WLR can deal with non-uniform mass and splitting naturally, at its current stage, it is not adapted to problems with unbalanced mass. Our work finds applications in single cell RNA analysis, see e.g. Schiebinger et al. [2019]. We don’t anticipate negative societal impacts.

## Acknowledgments and Disclosure of Funding

We thank the authors of Chewi et al. [2021] and Justiniano et al. [2023] for sharing their code with us. NS is partially supported by the NSF-BSF award 2019752 and the DFG award 514588180. CM is supported by NSF award DMS-2306064 and by a seed grant from the School of Data Science and Society at UNC. There are no competing interests to declare.

## References

- M. Agueh and G. Carlier. Barycenters in the wasserstein space. *SIAM Journal on Mathematical Analysis*, 43(2):904–924, 2011.
- L. Ambrosio, A. Bressan, D. Helbing, A. Klar, E. Zuazua, L. Ambrosio, and N. Gigli. A user’s guide to optimal transport. *Modelling and Optimisation of Flows on Networks: Cetraro, Italy 2009*, Editors: Benedetto Piccoli, Michel Rascle, pages 1–155, 2013.
- J.-D. Benamou, T. O. Gallouët, and F.-X. Vialard. Second-order models for optimal transport and cubic splines on the Wasserstein space. *Found Comp Math*, 19:113–1143, 2019. doi: 10.1007/s10208-019-09425-z.
- R. Cannoodt, W. Saelens, L. Deconinck, and Y. Saeys. Spearheading future omics analyses using dyngen, a multi-modal simulator of single cells. *Nature Communications*, 12(1):3942, 2021.
- A. Cavaretta, W. Dahmen, and C. Micchelli. *Stationary Subdivision*. Preprint / A: Fachbereich Mathematik. Freie Universität Berlin. Fachbereich Mathematik, 1989.
- Y. Chen, G. Conforti, and T. T. Georgiou. Measure-valued spline curves: An optimal transport viewpoint. *SIAM Journal on Mathematical Analysis*, 50(6):5947–5968, 2018.
- S. Chewi, J. Clancy, T. Le Gouic, P. Rigollet, G. Stepaniants, and A. Stromme. Fast and smooth interpolation on Wasserstein space. In *International Conference on Artificial Intelligence and Statistics*, pages 3061–3069. PMLR, 2021.
- J. Clancy and F. Suarez. Wasserstein-Fisher-Rao splines. arXiv:2203.15728, 2022.
- N. Courty, R. Flamary, A. Habrard, and A. Rakotomamonjy. Joint distribution optimal transportation for domain adaptation. *Advances in neural information processing systems*, 30, 2017.
- K. Craig, K. Elamvazhuthi, and H. Lee. A blob method for mean field control with terminal constraints. *arXiv preprint arXiv:2402.10124*, 2024.
- M. Cuturi. Sinkhorn distances: Lightspeed computation of optimal transport. In C. J. C. Burges, L. Bottou, M. Welling, Z. Ghahramani, and K. Q. Weinberger, editors, *Advances in Neural Information Processing Systems 26*, pages 2292–2300. Curran Associates, Inc., 2013.
- N. Dyn and N. Sharon. Manifold-valued subdivision schemes based on geodesic inductive averaging. *Journal of Computational and Applied Mathematics*, 311:54–67, 2017a. doi: 10.1016/j.cam.2016.07.008.
- N. Dyn and N. Sharon. A global approach to the refinement of manifold data. *Mathematics of Computation*, 86(303):pp. 375–395, 2017b.
- N. Dyn and N. Sharon. Improving the convergence analysis of linear subdivision schemes. <https://arxiv.org/abs/2405.09414>, 2024.
- N. Dyn, D. Levin, and J. A. Gregory. A 4-point interpolatory subdivision scheme for curve design. *Computer Aided Geometric Design*, 4(4):257–268, 1987. ISSN 0167-8396. doi: [https://doi.org/10.1016/0167-8396\(87\)90001-X](https://doi.org/10.1016/0167-8396(87)90001-X).
- R. Flamary, N. Courty, A. Gramfort, M. Z. Alaya, A. Boissunon, S. Chambon, L. Chapel, A. Corenflos, K. Fatras, N. Fournier, et al. Pot: Python optimal transport. *Journal of Machine Learning Research*, 22(78):1–8, 2021.



- N. Howe, S. Dufort-Labbé, N. Rajkumar, and P.-L. Bacon. Myriad: a real-world testbed to bridge trajectory optimization and deep learning. *Advances in Neural Information Processing Systems*, 35:29801–29815, 2022.
- X. Huang, Y. Wang, V. Guizilini, R. Ambrus, A. Gaidon, and J. Solomon. Representation learning for object detection from unlabeled point cloud sequences. In *Conference on Robot Learning*, 2022.
- G. Huguet, D. S. Magruder, A. Tong, O. Fasina, M. Kuchroo, G. Wolf, and S. Krishnaswamy. Manifold interpolating optimal-transport flows for trajectory inference. *Advances in Neural Information Processing Systems*, 35:29705–29718, 2022.
- J. Justiniano, M. Rumpf, and M. Erbar. Approximation of splines in Wasserstein spaces. *arXiv preprint arXiv:2302.10682*, 2023.
- L. V. Kantorovich. On the translocation of masses. *Journal of Mathematical Sciences*, 133(4): 1381–1382, 2006.
- J. M. Lane and R. F. Riesenfeld. A theoretical development for the computer generation and display of piecewise polynomial surfaces. *IEEE Transactions on Pattern Analysis and Machine Intelligence*, PAMI-2(1):35–46, 1980. doi: 10.1109/TPAMI.1980.4766968.
- J. Lott. Some geometric calculations on Wasserstein space. *Comm. Math. Phys.*, 277:423–437, 2008.
- K. R. Moon, D. Van Dijk, Z. Wang, S. Gigante, D. B. Burkhardt, W. S. Chen, K. Yim, A. v. d. Elzen, M. J. Hirn, R. R. Coifman, et al. Visualizing structure and transitions in high-dimensional biological data. *Nature biotechnology*, 37(12):1482–1492, 2019.
- F. Otto. The geometry of dissipative evolution equations: the porous medium equation. *Comm. Partial Differential Equations*, 26(1-2):101–174, 2001. doi: 10.1081/PDE-100002243.
- G. Peyré, M. Cuturi, et al. Computational optimal transport: With applications to data science. *Foundations and Trends® in Machine Learning*, 11(5-6):355–607, 2019.
- W. Saelens, R. Cannoodt, H. Todorov, and Y. Saeys. A comparison of single-cell trajectory inference methods. *Nature biotechnology*, 37(5):547–554, 2019.
- F. Santambrogio. Optimal transport for applied mathematicians. *Birkhäuser, NY*, 55(58-63):94, 2015.
- G. Schiebinger, J. Shu, M. Tabaka, B. Cleary, V. Subramanian, A. Solomon, J. Gould, S. Liu, S. Lin, P. Berube, et al. Optimal-transport analysis of single-cell gene expression identifies developmental trajectories in reprogramming. *Cell*, 176(4):928–943, 2019.
- Y. Sha, Y. Qiu, P. Zhou, and Q. Nie. Reconstructing growth and dynamic trajectories from single-cell transcriptomics data. *Nature Machine Intelligence*, pages 1–15, 2023.
- A. Tong, J. Huang, G. Wolf, D. Van Dijk, and S. Krishnaswamy. TrajectoryNet: A dynamic optimal transport network for modeling cellular dynamics. In *International conference on machine learning*, pages 9526–9536. PMLR, 2020.
- C. Villani. *Optimal Transport: Old and New*, volume 338. Springer Science & Business Media, 2008.
- J. Wallner and N. Dyn. Convergence and  $C^1$  analysis of subdivision schemes on manifolds by proximity. *Computer Aided Geometric Design*, 22(7):593–622, 2005. doi: 10.1016/j.cagd.2005.06.003.

## A Subdivision Schemes and Extension of WLR

We briefly describe subdivision schemes and their adaptation to the nonlinear domain via nonlinear averaging. Given an ordered sequence of points,  $\mathbf{p} = \{p_i\}_{i=0}^T \subset \mathbb{R}^d$ , we consider a linear *refinement rule* of the form

$$S(\mathbf{p})_j = \sum_{i \in \mathbb{Z}} a_{j-2i} p_i, \quad j \in \mathbb{Z}, \quad (5)$$

where  $\{a_i\}_{i \in \mathbb{Z}} \subset \mathbb{R}$  is the *mask* of the refinement rule  $S$ . We assume the mask has finitely many non-zero elements, that is,  $|I| < \infty$ . Note that to avoid any technical boundary treatment, we extend the sequence  $\mathbf{p}$  to all of  $\mathbb{Z}$  by repeating the starting point  $p_0$  and the endpoint  $p_T$ , i.e., we consider  $\dots, p_0, p_0, p_1, \dots, p_{T-1}, p_T, p_T, \dots$

To obtain finer and finer sequences of  $\mathbf{p}$ , we consider  $S^k(\mathbf{p})$ , i.e.  $S$  is applied  $k$ -times to  $\mathbf{p}$ . The repeated application of refinement rules is called a subdivision scheme. A subdivision scheme is called *convergent* if the piecewise linear interpolant to the data  $(i2^{-k}, S^k(\mathbf{p})_i)$  converges uniformly to a continuous limit curve with values in  $\mathbb{R}^d$ . See Cavaretta et al. [1989] for more details.

It has been observed in [Wallner and Dyn, 2005, Theorem 1] that any affinely invariant ( $\sum_i a_{j-2i} = 1$  for all  $j$ ) refinement rule as in (equation 5) can be (non-uniquely) expressed via the averaging operator  $\text{av}$  from eq. (3). Wallner and Dyn [2005] further observed that this fact can be used to define refinement rules for sequences  $\mathbf{p}$  in Riemannian manifolds by replacing  $\text{av}$  by the geodesic average.

While we discuss the Lane-Riesenfeld algorithm (Section 3) as the main algorithm in this paper, and we mention the 4-point scheme as an interpolatory alternative in Appendix A.1, we would like to point out that the idea presented in Section 3 naturally extends to all subdivision schemes. Therefore, replacing  $\text{av}$  in any subdivision scheme by OT- $\text{av}$  gives rise to a large set of interpolatory and approximating schemes in the Wasserstein space. We choose WLR to showcase this idea and because it can flexibly adapt to different smoothness degrees (through the parameter  $M$ ) and has strong convergence properties as presented in Dyn and Sharon [2017a,b], which we extend in Section 3.2 and Appendix C.

### A.1 Four Point Scheme

We showcase an interpolatory alternative to WLR, which is built from the 4-point scheme of Dyn et al. [1987]. The algorithm is presented in Algorithm 4, and is built from the original 4-point scheme by replacing linear averages with OT- $\text{av}$ . An example on two-dimensional circular non-uniform Gaussian data is presented in Figure 4.

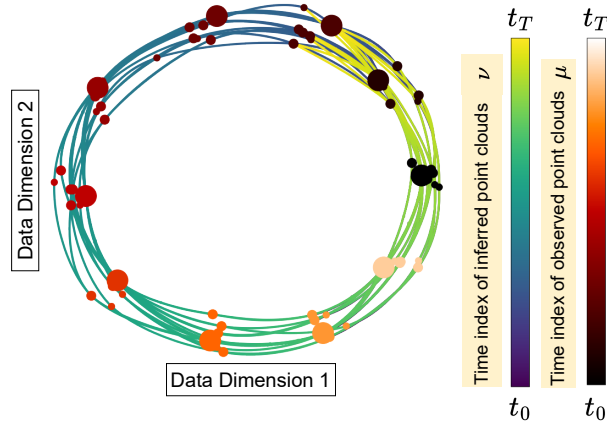


Figure 4: Exact interpolation via the Wasserstein Four Point Scheme.

## B Runtime Analysis

The runtime results in Figure 5 were obtained by running WLR for varying degrees ( $M$ ) and refinement levels ( $R$ ) on the Diverging Gaussian dataset. It is evident that the runtime increases

---

**Algorithm 4** 4-Point Scheme in Wasserstein Space

---

```

1: procedure FOURPOINTSHEME( $[\mu_{t_j}]_{j=0}^T, R$ )
2:   input Point clouds to be refined  $[\mu_{t_j}]_{j=0}^T$ .
3:   input Refinement level  $R \in \mathbb{Z}_+$ .
4:    $\nu^{(0)} \leftarrow [\mu_{t_j}]_{j=0}^T$ 
5:    $w \leftarrow \frac{1}{16}$   $\triangleright w$  is weighted averaging parameter
6:   for  $r = 1$  to  $R$  do
7:     for  $j = 2$  to  $(|\nu^{(r-1)}| - 1)$  do
8:        $\nu_{2j}^{(r-1)} \leftarrow \nu_j^{(r-1)}$ 
9:     end for
10:    for  $j = 2$  to  $(|\nu^{(r-1)}| - 2)$  do
11:       $X_A \leftarrow \text{OT-AV}(\nu_j^{(r-1)}, \nu_{j-1}^{(r-1)}, -2w)$ 
12:       $X_B \leftarrow \text{OT-AV}(\nu_{j+1}^{(r-1)}, \nu_{j+2}^{(r-1)}, -2w)$ 
13:       $\nu_{2j+1}^{(r)} \leftarrow \text{OT-AV}(X_A, X_B, \frac{1}{2})$ 
14:    end for
15:     $\nu^{(r)} \leftarrow [\nu_4^{(r)}, \dots, \nu_{2(|\nu^{(r-1)}|-1)}^{(r)}]$ 
16:  end for
17:  return Refined point clouds  $\nu^{(R)}$ .
18: end procedure

```

---

significantly as  $R$  increases, particularly beyond  $R = 7$ . While  $M$  also influences runtime, its impact is less pronounced. This is consistent with our analysis in Section 3.1 that complexity grows exponentially with  $R$  and linearly with  $M$ . In practice,  $R = 7, M = 3$  is more than enough to achieve smooth trajectories in most cases.

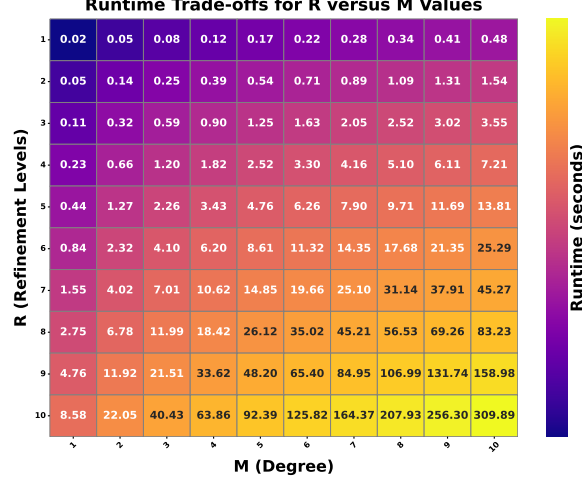


Figure 5: WLR runtimes on the Diverging Gaussian dataset with varying degrees and refinement levels.

## C Convergence Guarantees for WLR

The convergence result of Theorem 1 follows from adapting the results of Dyn and Sharon [2017b] to the Wasserstein setting. Our main insight is that while the proofs in Dyn and Sharon [2017b] are stated for finite-dimensional Riemannian manifolds, they naturally extend to the Wasserstein space. The reason is that the  $p$ -Wasserstein distance has the geodesic property, see eq. (4), and that it is a complete metric space.

We now present an outline of the proof, emphasizing the main arguments and using the notation of this paper.

First, we recall the notion

$$\Delta\nu^{(R)} := \sup_{j \in \mathbb{Z}} W_p(\nu_j^{(R)}, \nu_{j+1}^{(R)}), \quad (6)$$

and assume that the initial data is bounded, that is,  $\Delta\nu^{(0)} < \infty$ . Following the arguments in the proof of Dyn and Sharon [2017b], we get that there exist  $\eta \in (0, 1)$  such that

$$\Delta\nu^{(R)} \leq \eta \Delta\nu^{(R-1)}, \quad R \in \mathbb{N}.$$

We term the factor  $\eta$  *contractivity factor*. Using the geodesic property of eq. (4), one can actually show that WLR has a contractivity factor of  $\eta = 1/2$ . In fact, this value equals the contractivity factor of the original linear Lane-Riesenfeld scheme, which is the optimal contractivity for linear subdivision schemes, see Dyn and Sharon [2024].

To follow the proof of Dyn and Sharon [2017b], we also need an additional mild condition, the *displacement-safe property*, which is immediately satisfied for WLR, because it is satisfied for the standard linear Lane-Riesenfeld algorithm. This, together with the contractivity property, implies that there exists a constant  $C$ , independent of  $R$ , such that  $W_p(N^{(R+1)}(t), N^R(t)) \leq C\eta^R$ . And so the convergence follows since for any  $\ell \in \mathbb{N}$  we have

$$W_p(N^{(R+\ell)}(t), N^R(t)) \leq C\eta^R(1 + \eta + \dots + \eta^\ell) \leq \frac{C}{1 - \eta}\eta^R.$$

Namely,  $\{N^{(R)}(t)\}_{R \in \mathbb{Z}_+}$  is a Cauchy sequence in the Wasserstein space, and since this space is complete, the sequence converges to a limit.

## D Additional Results

We present full visual comparison between WLR and other methods in Figure 6. Trajectory inference is done on all timesteps with no hold-out point clouds.

## E Experimental Details

We provide details on the experiments in Section 4. All experiments including runtime calculations were carried out on x86\_64 machine with AMD EPYC 7713 64-Core Processor with NVIDIA A100-PCIE-40GB GPU. WLR, F&S and Wasserstein-Fisher-Rao did not require any GPU for training. Our paper used two software packages: Python OT<sup>3</sup> version 0.9.3 with MIT license from Flamary et al. [2021] and Dyngen<sup>4</sup> version 1.0.5 with MIT license (CC-BY) from Cannoodt et al. [2021]. Dataset details are in Table 2.

Dataset	Dimension $d$	Timesteps $T + 1$	Number of points $n_t$	Author
Diverging Gaussian	2	4	200	Us
Petal	2	5	135	Huguet et al. [2022]
Converging Gaussian	2	4	32, 96, 64, 32	Clancy and Suarez [2022]
Dyngen Tree	10	7	319	Cannoodt et al. [2021]
Dyngen Cycle	10	15	52	Cannoodt et al. [2021]

Table 2: Details on the synthetic datasets used in Section 4.

**Wasserstein Lane-Riesenfeld (WLR)** We used  $M = 10$  for Petal and  $M = 2$  for the rest.  $R = 7$  in all experiments.

**TrajectoryNet** For all experiments, we used TrajectoryNet<sup>5</sup> with 1000 iterations and `whiten=True` with all other default optimization parameters in Tong et al. [2020].

<sup>3</sup><https://pythonot.github.io/>

<sup>4</sup><https://github.com/dynverse/dyngen>

<sup>5</sup><https://github.com/KrishnaswamyLab/TrajectoryNet>

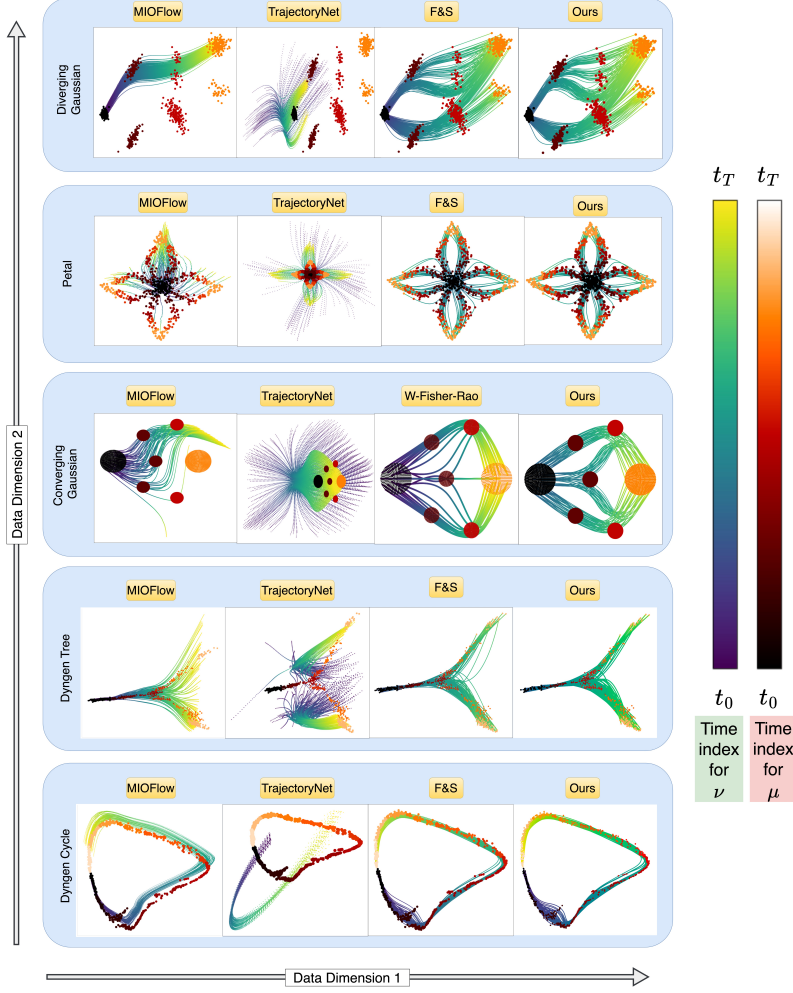


Figure 6: Full-scale visual comparison between WLR and other methods.

**MIOFlow** We observed the best trajectory inference results without training the geodesic autoencoder but utilizing the density loss for all of our experiments. We used the following hyperparameters for MIOFlow<sup>6</sup>. Despite our best efforts, we were unable to reproduce their published figure on Petal. After multiple attempts, we report their *best* outcome in Table 1 and Figure 6.

- Diverging Gaussian: sample\_size=60, n\_local\_epochs = 50, n\_epochs = 0, n\_post\_local\_epochs = 0,  $\lambda_e = 0.001$ ,  $\lambda_d = 10$ ,  $\epsilon = 0.5$  n\_points = 200, n\_trajectories = 200, n\_bins = 500, n\_epochs\_emb = 1000
- Converging Gaussian: sample\_size=30, n\_local\_epochs = 50, n\_epochs = 0, n\_post\_local\_epochs = 0,  $\lambda_e = 0.001$ ,  $\lambda_d = 35$ ,  $\epsilon = 0.5$  n\_points = 64, n\_trajectories = 64, n\_bins = 500, n\_epochs\_emb = 1000
- Petal: n\_local\_epochs = 50, n\_points = 135, n\_trajectories = 135, n\_bins = 500. The rest are default hyperparameters mentioned in Huguet et al. [2022].
- Dyngen Tree: sample\_size=30, n\_local\_epochs = 5, n\_epochs = 0, n\_post\_local\_epochs = 0,  $\lambda_e = 0.001$ ,  $\lambda_d = 15$ ,  $\epsilon = 0.5$  n\_points = 100, n\_trajectories = 100, n\_bins = 500, n\_epochs\_emb = 1000
- Dyngen Cycle: sample\_size=30, n\_local\_epochs = 10, n\_epochs = 0, n\_post\_local\_epochs = 0,  $\lambda_e = 0.001$ ,  $\lambda_d = 15$ ,  $\epsilon = 0.5$  n\_points = 50, n\_trajectories = 50, n\_bins = 500, n\_epochs\_emb = 1000

<sup>6</sup><https://github.com/KrishnaswamyLab/MIOFlow>

**Fast and Smooth (F & S)** The original authors of Chewi et al. [2021] proposed a general algorithm for performing interpolation using cubic splines in  $\mathbb{R}^d$  after determining an ordering through successive optimal transport computations on the initially observed point clouds. To ensure a fair comparison, we wrote our own code to adapt their methodology to approximate B-splines in  $\mathbb{R}^d$  via the Lane-Riesenfeld algorithm. We used the same  $M$  and  $R$  as WLR. As mentioned in Section 4.1, F&S is not able to run on Converging Gaussian.

**Wasserstein-Fisher-Rao** The authors of Clancy and Suarez [2022] proposed a method for computing splines for measures of differing masses using the notion of unbalanced optimal transport. We used their method for computing splines on the converging Gaussian data using all default parameters with  $\eta_{\text{OT}} = 0.001$  for 200 iterations and 32 interpolating splines from the first to the last timestep. As mentioned in Section 4.1, we were able to run their code<sup>7</sup> only on this dataset.

---

<sup>7</sup>[https://github.com/felipesua/WFR\\_splines](https://github.com/felipesua/WFR_splines)